Masterthesis

Investigation of fatigue ductile-brittle transition in steel and welded joints.

by

Finn Sallaba

Supervisors: Prof. DSc. (Tech.) Sören Ehlers
D.Sc. (Tech.) R. U. Franz von Bock und Polach
Moritz Braun, M.Sc.

Institute for Ship Structural Design and Analysis (M-10)
Hamburg University of Technology

Hamburg, January 2020

Declaration of Originality

Hamburg, 30.01.2020

I, Finn Sallaba, certify that the work presented here is, to the best of my knowledge and belief, original and the result of my own investigations, except where otherwise indicated. It has not been submitted, either in part or whole, for a degree at this or any other University.

Finn Sallaba

Abstract

This work presents a partitioned approach to fluid-structure interaction problems in analyses of blood flow in aneurysm (cardiovascular disease) considering the surrounding human tissue. The surrounding tissue is represented as an elastic foundation, which provides the tractions due to the displacement of the structure model. The influence of the elastic bedding to the behavior of the structure and fluid is analysed considering aneurysms of different shapes. The analyses show, that the elastic bedding affects the structural behavior, which changes the blood flow significantly. The three subproblems fluid, structure and surrounding tissue are coupled using a partitioned solution approach.

TUHH
Technische Universität Hamburg

Konstruktion
und Festigkeit
von Schiffen

TUHH · M-10 · Am Schwarzenberg Campus 4C · D-21073 Hamburg

MASTER THESIS DESCRIPTION

for

Finn Sallaba

Investigation of fatigue ductile-brittle transition in steel and welded joints (Deutsch: Untersuchungen des duktil-spröden Übergangsverhalten von Ermüdungsrisswachstum in Stahl und Schweißverbindungen)

The formation and propagation of cracks occurs through non-deflectable dislocation movements at notches, material defects and grain boundaries. Since this process is partly thermally controlled, the resistance to dislocation movements at low temperatures increases. This slows both fatigue initiation and fatigue crack propagation. From recent experimental data it can be seen that fatigue crack growth is accelerated below a transition temperature (termed fatigue transition temperature (FTT)) that correlates with the ductile-brittle transition temperature (DBTT) found by well-known fracture mechanics tests, i.e. Charpy impact, fracture toughness and CTOD. In general, more research is required to measure the FTT by means of fatigue crack growth rate tests. Since measuring the fatigue crack growth with electrical-magnetic methods requires high precision measurement methods, such tests need to be carefully calibrated. For this purpose, the crack growth rates in welded and base material specimens will be measured over a range of temperatures. Hence, this project is concerned with the measurement of fatigue crack growth rates at sub-zero temperatures. For this purpose, the direct current potential drop method will be applied. The work consists of:

1) Calibration of the direct current potential drop method for fatigue crack growth rate tests with notched middle tension specimen at sub-zero temperatures
2) Crack growth rate curves shall be measured on notched middle tension specimen before and after welding at based on the relevant industry standards
3) The test results shall be analysed regarding the effect of temperature on fatigue crack growth rates and be compared with published data

Literature studies of specific topics relevant to the thesis work shall be included.

The work scope may prove to be larger than initially anticipated. Subject to approval from the supervisors, topics may be deleted from the list above or reduced in extent.

In the thesis the candidate shall present his personal contribution to the resolution of problems within the scope of the thesis work.

Theories and conclusions should be based on mathematical derivations and/or logic reasoning identifying the various steps in the deduction.

The candidate should utilise the existing possibilities for obtaining relevant literature.

Thesis format
The thesis should be organised in a rational manner to give a clear exposition of results, assessments, and conclusions. The text should be brief and to the point, with a clear language and the objective to be published in a conference article and/or scientific journal. It is thus desirable that the thesis is written in English. Telegraphic language should be avoided.

The thesis shall contain the following elements: An executive summary, list of symbols and acronyms, followed by the main body of the thesis consisting of a brief background introduction, a state of the art defining the knowledge gaps defining the scope or work and limitations, the actual contribution chapters, conclusions with recommendations for further work, references and (optional) appendices. All figures, tables and equations shall be numerated.

The supervisors require that the candidate, in an early stage of the work, presents a written plan for the completion of the work. The plan may include a budget for the use of computer and laboratory resources if applicable, which will be charged to the department. Overruns shall be reported to the supervisors.

The original contribution of the candidate and material taken from other sources shall be clearly defined following basic academic principles and an acknowledged referencing system, which includes the name of the referred authors followed by the publication year in the text. The subsequent reference list can thus be alphabetical.

The report shall be submitted in two copies:
- Signed by the candidate
- The text defining the scope included
- In bound volume(s)
- Drawings and/or computer prints, which cannot be bound should be organised in a separate folder.
- The report shall also be submitted in PDF along with essential input files for computer analysis, spread sheets, MATLAB files etc. in digital format.

Ownership
According to the current rules, the candidate has the ownership of the thesis. Any use of the thesis has to be approved by TUHH M-10 (or external partner when this applies). TUHH M-10 has the right to use the thesis as if a TUHH M-10 employee carried out the work, if nothing else has been agreed in advance.

Thesis supervisors
Prof. D.Sc. (Tech.) Sören Ehlers, D.Sc. (Tech.) Franz von Bock und Polach, Moritz Braun

Deadline: 30.01.2020

Hamburg, 30.07.2019

Danksagung

Ein besonderer Dank gilt meinem Betreuer Moritz Braun, der mir in fachlichen Fragen zur Seite gestanden hat und mir bei der Durchführung der Versuche weitgehend freie Hand gelassen hat. Für die Nutzung der

Contents

List of Figures

List of Tables

Acronyms

BS	British Standards
DC	direct current
CDG	Crack Detection Gauges
DBTT	Ductile Brittle Transition Temperature
M(T)	Middle tension
TUHH	Hamburg University of Technology
FTT	Fatigue Transition Temperature
FDBT	Fatigue Ductile Brittle Transition
DBT	Fracture Ductile to Brittle Transition
SIF	Stress intensity factor (range)

List of Symbols

Symbol	Unit	Meaning
a	mm	Crack length
a_R	mm	Initial crack length
C	-	Paris equation constant
da/dN	mm/cycle	Fatigue crack growth rate
K	MPa$\sqrt{\text{m}}$	Stress intensity factor
K_C	MPa$\sqrt{\text{m}}$	Stress intensity factor of final failing
P_{max}	N	Maximum force
P_{min}	N	Minimum force
m	-	Paris equation constant
R	-	Stress ratio
S_{max}	N	Maximum stress
S_{min}	N	Minimum stress
$T_{loadcell}$	°C	Temperature of the load cell
V	mV	Actual potential voltage
V_R	mV	Initial potential voltage
W	mm	Width of specimen
Y_I	mm	Distance current input pin to crack plane
Y_R	mm	Distance reference current measuring bolt to crack plane
Y_0	mm	Distance measuring pin to crack plane
α	-	Normalized crack length
β	-	Dimensionless geometry factor
Δa_{cdg}	mm	length correction of DCG
ΔK	MPa$\sqrt{\text{m}}$	Stress intensity factor range
ΔK_{max}	MPa$\sqrt{\text{m}}$	critical value stress intensity factor range
ΔK_{th}	MPa$\sqrt{\text{m}}$	Threshold value stress intensity factor range
ΔP	N	Force range
ΔS	N/m^2	Stress range
$\sigma_{O,X,Y}$	N/m^2	Local stresses
$\tau_{yx,xz,zx}$	N/m^2	

Chapter 1

Introduction

The interest for exploring the arctic region has been very keen for years, however recently it increased even more.

The main reason for higher activities is the higher mean temperature caused by the climate change. In 2007 the European Space Agency with use of satellite measurements registered the decrease of area of ice to 3M square meters, which was the lowest in the history of measurements back then [14]. The national snow and ice data center recorded a ice extend within the last 10 years in the arctic which is way lower than the meridian of former 20 years. [25]
It was registered that North West Passage opened creating the possibility to navigate from Atlantic to Pacific along the coasts of Canada. This route is by far shorter than the routes ships had to sail so far.
Another effect of reduced thickness of the ice and melting permafrost ground which may allow access in the nearby future to the extensive natural resources of Arctica. By using a probabilistic geology-based methodology the United States Geological Survey assessed the size of oil and gas resources in the area north of the Arctic Circle. It was estimated that about 30% of the world's undiscovered gas and 13% of the world's undiscovered oil may be found there, mostly offshore under less than 500 meters of water [18].
Nevertheless the condition in Arctic regions can be still very tough. Ships and other structures made from steel will be exposed to very low temperature which are highly unfavourable due to the negative impact on the material. The safety of the persons working on and protection of the nature are of highest priority. Because of the conditions in arctic regions von Bock und Polach et al.[4] has identified fatigue at low temperatures as a major point of interest of future science and a knowledge gap. The activity in research on material behaviour in fatigue has increased steadily in recent years. Investigations of the fatigue properties of steel and welded joints at low temperatures have moved into focus of scientific investigations. [7],[5],[8],[23]

Scope of this thesis are investigations of M(t) Specimen made from S500 steel and welded joints in crack growth experiments at room temperature and and low temperatures. The

aim of the thesis is a better comprehension of the relationship of fracture and fatigue ductile to brittle transition.

Chapter 2

State of the art

A short introduction of the most important theory topics of this work is given in this chapter.

2.1 Cyclic loading

Fatigue tests are often performed with constant amplitudes and maximum and minimum load levels. The constant amplitude loading is owning some characteristic parameters which are shown in figure 2.1. The amplitude σ_a is defined as the difference between the maximum and minimum stress of a cycle. The definition of maximum and minimum stress are shown in the equations 2.3.

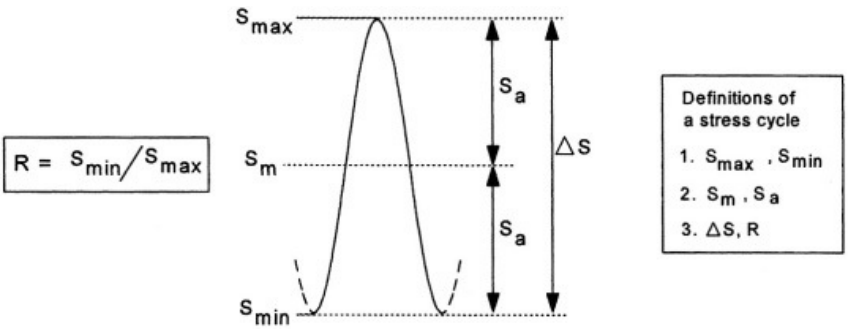

Figure 2.1 Significant values of load cycles, with other notation. S is corresponding to σ in the text. The Figure is taken from [27].

$$\sigma_a = \frac{\Delta\sigma}{2} = \frac{\sigma_{max} - \sigma_{min}}{2} \tag{2.1}$$

The mean stress is defined as the average of the maximum and minimum stress. [11]

$$\sigma_m = \frac{\sigma_{max} + \sigma_{min}}{2} \tag{2.2}$$

Mode I	opening mode
Mode II	sliding mode
Mode III	tearing mode

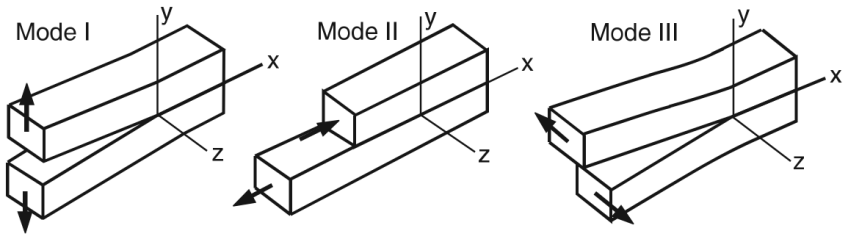

Figure 2.2 Crack opening modes [11]

$$\sigma_{max} = \sigma_m + \sigma_a \qquad \sigma_{min} = \sigma_m - \sigma_a \tag{2.3}$$

2.2 Stress ratio

The stress ratio R is defined as the fraction of the minimum and the maximum stresses [17].

$$R = \frac{\sigma_{min}}{\sigma_{max}} \tag{2.4}$$

2.3 Crack opening modes

Depending on the acting loads the displacement of the crack surfaces will be different. The crack opening modes can be divided into three cases, which can occur individually as well as together.

In Mode I the forces are opening the crack by moving faces apart from each other. Mode II is called sliding mode, the forces are acting perpendicular to the front end and the surfaces are sliding on each other. The third mode is named tearing mode, the forces are acting in the plane of the crack as well. The crack surfaces are sliding on each other by the force in the plane of the front end. [27]
All the three Modes were presented in Figure 2.2. For the experiments of this thesis Mode I is primary of interest.

2.4 Stress intensity factor

Stress intensity factor characterises the severity of stresses in the tip of the crack. The idealised presumption is a sharp crack tip and linear elastic and isotropic material. The

stress state in the crack tip is represented by the following stresses: $\sigma_x, \sigma_y, \tau_{xy}$.

$$\sigma_x = \frac{K}{\sqrt{2\pi r}} cos\frac{\theta}{2}(1 - sin(\frac{\theta}{2})sin(\frac{3\theta}{2})) \tag{2.5}$$

$$\sigma_y = \frac{K}{\sqrt{2\pi r}} cos\frac{\theta}{2}(1 - sin(\frac{\theta}{2})sin(\frac{3\theta}{2})) \tag{2.6}$$

$$\tau_{xy} = \frac{K}{\sqrt{2\pi r}} cos\frac{\theta}{2}sin(\frac{\theta}{2})sin(\frac{3\theta}{2}) \tag{2.7}$$

with:

$$K = \beta S\sqrt{\pi a} \tag{2.8}$$

K is the severity of the stress intensity, β the dimensionless geometry factor. The crack length is a, external loads causing the nominal stress S. The stress decreasing in correlation of the distance to the crack tip is characterised by $1/\sqrt{\pi r}$. K is the characteristic parameter for the stress intensity in the area of the crack tip. [27]

2.5 Three stages of crack growth

Depending on the level of the stresses during the cycling testing the speed of crack growth is changing. For very high stresses the crack growth is very fast or the specimen is braking suddenly. For moderate stresses the change in crack growth rates can be better estimated for a slight increase or decrease of the loads. For very low stresses there is no crack propagation registered any more.
Diagram 2.3 is showing the relation between the crack growth per cycle da/dN and the stress intensity factor range ΔK in double logarithmic scales. In Figure 2.3 the three regions of the curve are shown. For this thesis only threshold and Paris region are of interest.

2.5.1 Threshold region

In the threshold region the crack is growing very slow. The threshold stress intensity factor ΔK_{th} is marking the stop of crack propagation. The curve runs asymptotically to this value, which is reached at a crack propagation da/DN of 10^{-10} m/cycle.

ASTM Standard E647 [13] defines this region in a range of the crack propagation da/dN between 10^{-9} m/cycle and 10^{-10} m/cycle.

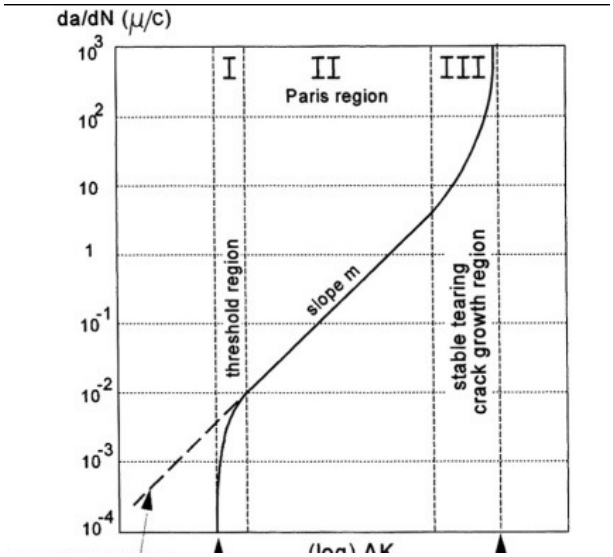

Figure 2.3 Three regions of crack growth. Taken from [27]

2.5.2 Paris region

For the Paris region the relation of da/dN and ΔK_{th} in logarithmic scales is linear. In Figure 2.3 the Paris region is marked by II. The Paris law is a power function which describes the crack growth da/dN by the material parameters C and m and the stress intesity factor range ΔK see equation 2.9.

$$da/dN = C(\Delta K)^m \tag{2.9}$$

2.5.3 Unstable crack growth

In the unstable crack growth region the crack is growing with 0.01 mm/cycle or even faster. In parts of the crack front the ductile tearing areas are treading. By reaching the critical stress intensity factor ΔK_C the specimen is breaking immediately. For very high crack growth rates the stress intensity factor is going asymptotic to this value.

2.6 Determination of the crack length

For determination of the crack length the following methods were used: beachmarks, crack detection gauges and the Johnson equation. Two of the methods provide continuous results on the current crack length during the test. The crack detection gauges shows the actual crack length at the surface, which may need to be corrected for accurate results. The Johnson Equation delivers the crack length during the whole experiment but requires necessarily the initial crack length at the beginning of the experiment. The evaluation of the beachmarks delivers exact crack length after the termination of the experiment.

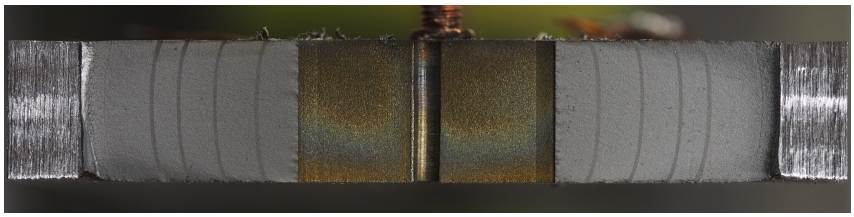

Figure 2.4 Beachmark of a center notched specimen

2.6.1 Direct Current Potential Drop-Method

The method uses the effect that the electrical potential of the sample changes with increasing crack length. For this purpose, current is passed through the sample and the voltage drop is measured across the crack.
The empirical Johnson-equation 2.10 set the normalized crack voltage in relation to the normalized crack length. The crack length is obtained by converting to equation 2.11.

$$\frac{V}{V_R} = \frac{cosh^{-1}(cosh(\frac{\pi y}{2W})/cos(\frac{\pi a}{2W}))}{cosh^{-1}(cosh(\frac{\pi y}{2W}/cos(\frac{\pi a_0}{2W})))} \tag{2.10}$$

$$a = \frac{W}{\pi} cos^{-1}(\frac{cosh(\frac{\pi}{W}Y_0)}{cosh(\frac{V}{V_R}cosh^{-1}(\frac{cosh(\frac{\pi}{W}Y_0)}{cos(\frac{\pi}{W}a_0)}))}) \tag{2.11}$$

The distance of the measuring pin to the crack plane is described by Y_0. The sample width is defined by W. In order to use the Johnson equation, the start-crack length a_0 and crack voltage V_R must be known at the start time. The current crack-voltage V can then be used for calculation of the crack length a.

2.6.2 Beach marks

Beach marks were created by changing the stress ratio R during the experiment. A ratio of R =0.75 led to the dark shaded lines shown in Figure 2.4.After the end of the experiment, the fracture surfaces were photographed and evaluated. The method recommended by ASTM E399-90 [12] was used to determine the crack length. The thickness of the specimen was split equidistant in four parts. Three points on the beachmark were used for the estimation of the crack length, see Figure 2.5. Point b was in the middle between point a and c, which were in equal distance between b and the surface of the specimen. The crack length was calculated by the mean values of a-c values. It describes the difference between the crack area determined midway between the beach marks and the crack length at the sample surface.??? For correction of the crack detection gauges the value Δa_{CDG} was estimated.

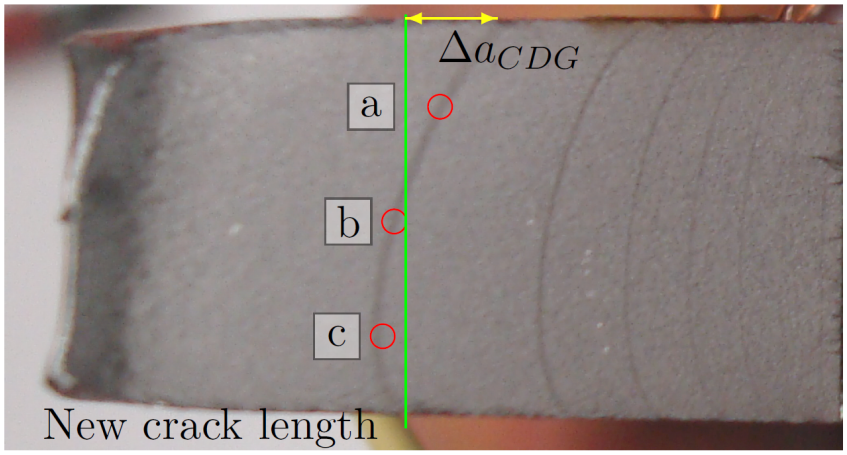

Figure 2.5 Evaluation of the crack length by beachmarks. [21]

2.6.3 Strain gauges

The crack detection gauges were glued to the surface of the specimen. The orientation was perpendicular to the machined notch and with a distance to the notch tip of 2mm. The exact position was estimated by the evaluation of a photography. The crack length was corrected by the values of Δa_{CDG}.
The corrected crack length was plotted and fitted. The fitted curves were used in the figures of the calibration curves. The crack detection gauges was also used for determination of the initial crack length of Johnson Equation.

2.7 Steel in cold enviroment

The process of transition from ductile to brittle fatigue behaviour is called fatigue ductile brittle transition (FDBT). The FDBT is characterised by a sudden increase in the crack growth rate falls below a certain temperature. The temperature at which the phenomena occurs is called Fatigue Transition Temperature (FTT).

This effect is known studied a lot for fracture and is called ductile brittle transition (DBTT).

2.8 Charpy impact test

For the Charpy method the impact energy is determined with a pendulum mechanism. The pendulum is dropped from a fixed height and the head of the pendulum hits the specimen which is fixed at the lowest point.The remaining energy after braking the specimen let the pendulum swing up on the other side . The height of the pendulum suspended above the lowest point is used to determine the impact energy.
The specimens of a material are tested for different temperatures. Depending on the

temperature of the specimen different fracture mechanisms occur. For stable crack propagation the fracture surface is characterized by a coarse surface and big plastic deformations of the specimen. The crack is growing relatively slow and much energy is absorbed by the plastic deformation. Unstable crack growth is marked by a smooth fracture surface almost without plastic deformations. The origin of the crack start is to be clearly identified. For the evaluation of the experiments for the same material but at different temperatures the results are plotted into the Charpy Impact Energy Transition curve. The Charpy energy is plotted over the temperature of the specimen.
The curve can be divided into three areas. Low temperatures lead to failure of the sample at low energy consumption. This responds to the unstable crack growth which is classified as brittle material behaviour. The consumed Charpy energy is low. For higher temperatures the material shows a ductile material behaviour characterized by stable crack growth. The consumed Charpy energy is higher. For temperatures in the range between a mixed form of cracks occur. For lower the brittle temperature the Charpy energy is nearly constant, this also applies for the Charpy energy for temperatures with ductile material properties.

2.9 Fatigue ductile brittle transition

According to present state of the art there is analogy between fatigue and fracture [30],[32]. The reduction f the temperature has an influence on the shape of the crack growth curve, what was presented in the Figure 2.6. The linear Paris region is shifted downwards for lower temperatures which are still above DBFT. The threshold values ΔK_{th} and ΔK_C are shifted to higher values. [1] This behaviour is similar to slow down of crack growth rate observed for lower temperatures.

When the temperature fall below the DBFT, the crack growth rate is showing a sudden change.[1]

The crack growth curve is shifted upward and change in the slope occur. [30] [1]

A bigger slope has an effect on the crack growth rate depending on the size of the SIF. Values between the intersection of the curve at temperature above FTT become smaller. values for bigger SIF than the intersection are becoming larger. Unlike most other authors Walters [30] reported a lower slope of the Paris fit for temperatures lower the FTT.

For the threshold values a change is reported too [30]. For temperature values between room temperature and FDBT the values of threshold SIF ΔK_{th} and critical SIF ΔK_C are shifted to higher values. The reduction of the temperature under FTT causes a way smaller ΔK_C.

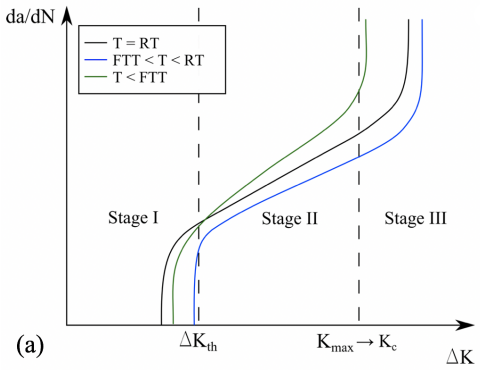

Figure 2.6 Schematic fatigue crack growth behaviour at different temperatures based on Alvaro [1]. Room temperature (black line) is compared with temperature below FDBT(green line) and between room temperature and FDBT (blue line).

Chapter 3

Equipment and setup

All experiments were performed at the lab of the Institute for Ship Structural Design and Analysis at Hamburg University of Technology (TUHH).
Subject of investigations was the crack propagation of center notched specimen made from S500 steel. Two types of specimens were part of the investigation. For first type the crack starter notch was placed in S500 base material.

The second type was made from S500 steel plate too but contained a welded joint. The starter notch for these specimens were placed in a the middle of the welded seam. The experiments for this work were carried out in a resonant testing machine, the specimens were tested in a temperature controlled chamber.

Scope of the investigations were the crack growth behaviour for low temperature. The experiments were performed with temperatures between ambient temperature and -110°C.

The specimen was clamped by two hydraulic clamps, which reach into the chamber. For the detection of the crack length the direct current potential drop method (DCPDM) was used.

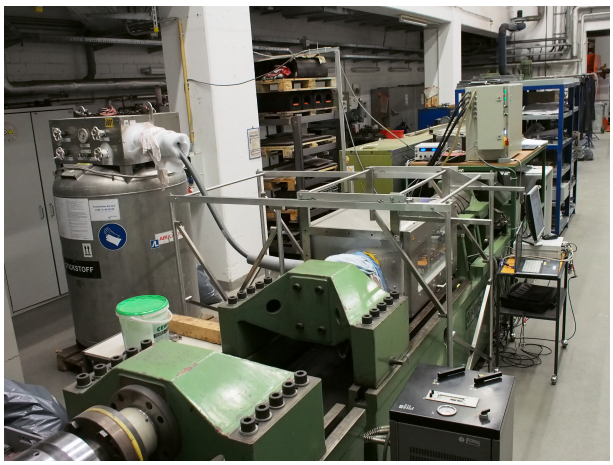

Figure 3.1 Experimental setup

3.1 Resonant testing equipment

The resonant testing machine is a dynamic testing machine for fatigue and crack propagation tests. A static load is applied to the specimen and superimposed with a dynamic load. The testing machine with the sample acts like a spring system, which is stimulated to vibrate. The system is controlled by a control unit produced by Ramull, which allows for programming of Load blocks and changing the load parameters of the testing machine.

The resonant testing machine was manufactured by Schenck. The entire test setup is shown in Figure 3.1.

3.2 Climate chamber

The climate chamber allows to run experiments in temperature controlled environment. For cooling nitrogen is vaporized inside the chamber and distributed by two fans.

A nitrogen storage tank of significant size supplies the chamber with liquid gas. The lowest possible temperature is limited by the vaporizing temperature of the nitrogen.

For heating an electrical heater is available. In present investigation it was used for defrosting and drying the chamber after experiments. The temperature inside the chamber is regulated by the Omron controller in a range from -180°C to 350 °C. The measuring cables are led out on the back of the chamber.

3.3 The design of the specimens

For the experiments two kind of middle tension M(t) specimens were used. Both specimen types were made from S500 steel. One type was made from homogenous material, the other one contained a but welded joint.

The blanks of the specimen were cut by a saw and subsequently further proceeded. The specimens had a longitudinal length of 500 mm. The width was 62-65 mm in the middle, on a length of 100 mm the specimens are wire eroded to a width of 58 mm. The transition from the tapered to the wider part was executed as a 50 mm radius. The thickness of the specimens were about 10 mm. The rolling direction of the steel corresponded to the longitudinal direction of the specimen. The base material specimen is shown in Figure 3.2

For a defined crack start a notch was machined into the specimen. The dimensions of the notch are shown in Figure 3.3a A bore was placed the middle of the specimen. Starting from the bore two 1mm wide slots with a length of 7.5 mm each were wire eroded. The slots were ending with an angle of 30 degrees.

The welded specimen have the same design as above, but have additional specifications. In the area where the sample has a width of 58 mm, the upper and lower sides of the specimen was additionally milled smooth. The thickness of this area amount 9.5 mm.

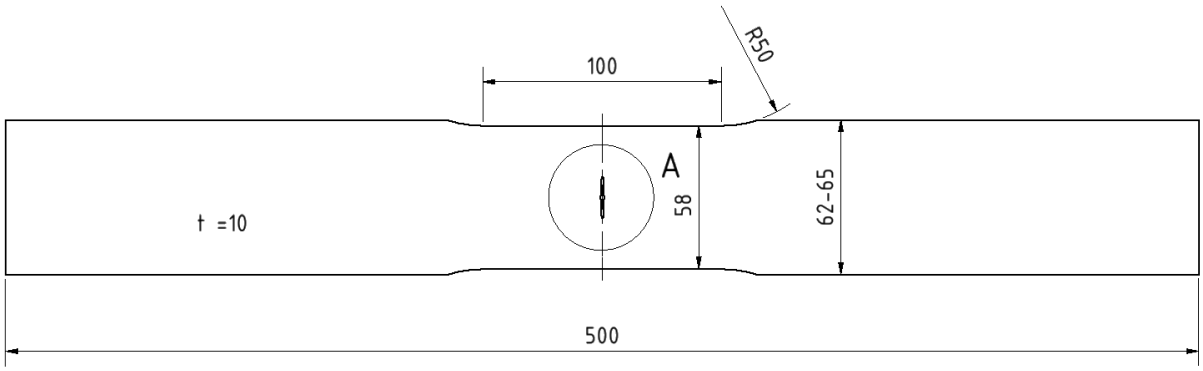

Figure 3.2 Design of the base material specimen.

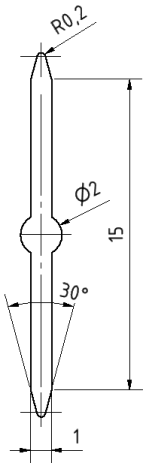

(a) **D**etail A: design of the notch

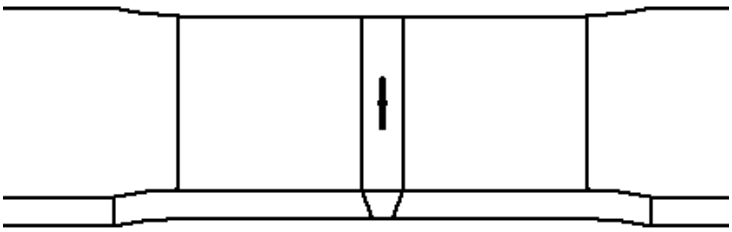

(b) **T**he notch at the welded specimen is placed in the same position as at the base material specimen. The notch was positioned centered and in the direction of the welded joint.

Figure 3.3 Calibration curves of S500 steel for the tested temperatures.

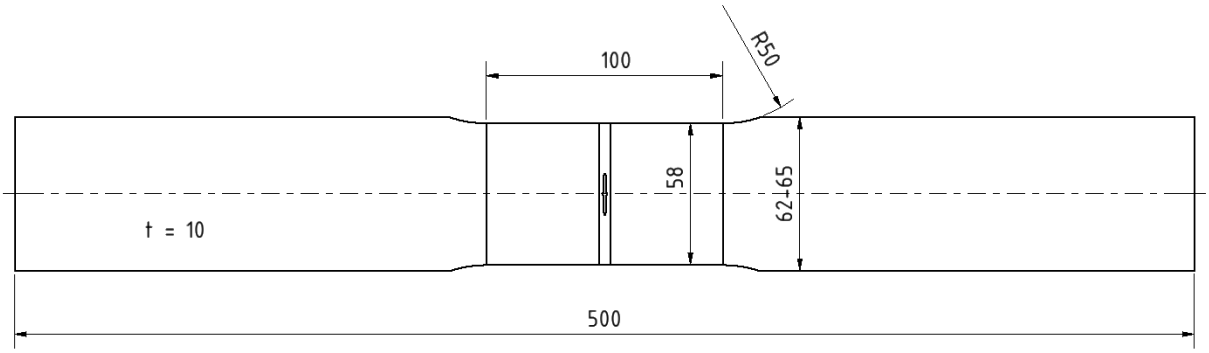

Figure 3.4 Design of the welded specimen with welded joint.

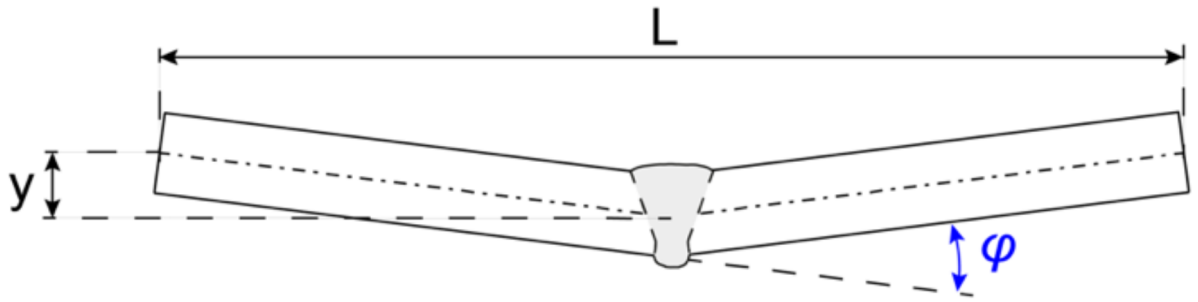

Figure 3.5 Angular misalignment of the welded specimens taken from [6]

The weld seam is positioned in a way that the notch is in the middle of it. This is shown in Figure 3.3b. The design of the welded specimen is shown in Figure 3.4.

The welding process causes distortions of the specimen. The angular misalignment is shown in Figure 3.5 The welding distortions of the tested specimen are shown in table 3.1.

Table 3.1 The misalignment of the welded specimens which were used for the experiments.

Experiment	Misalignment φ
Calibration curve RT	1.95°
Calibration curve -20 °C	0.88°
Calibration curve -50 °C	0.36°
Calibration curve -80 °C	1.04°
Const ΔK	0.24°
Decreasing ΔK	unknown

3.4 Electrical insulation of the specimens

The use of the direct current drop method requires that electric current is passed through the sample. To avoid contact of the specimen with electrical ground they were isolated from the hydraulic clamps. Resin circuit boards were put as isolation between the specimen and the clamps.

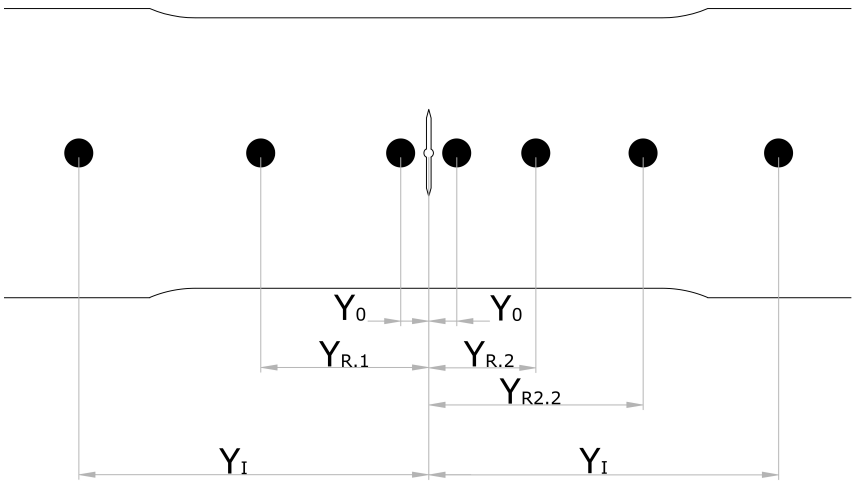

Figure 3.6 Positions of the welded bolts for measuring and current input cables taken from [15]

3.5 Insulation of electrical cables and temperature insulation

For connection of the cable with the specimen bolts were welded to the specimen. The bolts have an M3-thread and were covered with copper. Nuts were used to fix the soldered ring terminals of the cables.
The selections of the cables can have a big influence on the quality of the signal. For this reason the choice was made according to ASTM E647-15 [13]. The wiring have to be thick enough for transferring the current. On the other hand, it have to be thin enough to allow precise placement on the specimen and avoid stress through the cables. Application of thin cables are reducing the danger of breaking cables during the experiments. The best arrangement for the used test equipment had been figured out in former theses at TUHH by Hochfellner [21], Göpfrich [19] and Sallaba [15]. During the experiments at low temperatures it was found that by opening and closing the valve of the chamber the temperature in the chamber fluctuates. This fluctuations were causing a fast temperature change of the cables and was influencing the measured signals. To reduce the influence of this fluctuations on the measured results the cables inside the chamber were insulated by a hose made from air bubble film.

All bolts were placed in the middle of the width of the specimen, for exact placement stencils was used for welding. The current input bolts were placed on both sides of the notch in a distance of 75 mm. The measurement bolts for the crack current were placed in a distance of $Y_0 = 6$ mm to the notch. In a distance of Y_I =75 mm to both sides of the notch the bolts that are leading to the power supply unit are placed. For measuring of a reference current two bolts were placed on one equi-distant between one crack-current measuring bolt and one current input bolt. The positions of the bolts are shown in Figure 3.6

Table 3.2 Add caption

Symbol	Distance from notch to	Distance [mm]
Y_0	measurement bolts for crack current	6
Y_I	current input pins	75
Y_{R1}	not used any more	
Y_{R2}	measurement bolts for reference current	46

3.6 Measurement amplifier

The Peekel Autolog 3000 amplifier was used for the experiments. The Autosoft 3000 software was used for recording the data. The physical channels of the Autolog 3000 have a clock of 1kHz. Virtual channels can be used to perform simple calculations with the measured values. The clock does not have to correspond to the clock of the measuring amplifier. The measured values of the experiment were processed and stored in Autosoft. The memory clock was 6 seconds, what had been figured out as a good mean time in a former work [15]. After finishing the experiment following values were exported to a text-file. In table 3.3 a list of the recorded channels is shown. The values of the stress intensity factor ΔK and the Johnson crack length can be observed during the experiment. For final evaluation of the experiments they were calculated separately.

Table 3.3 List of recorded channels, that are written to text-file by export of the experiment data.

channel	type of value
date and time	
number of load cycles	quantity
Frequency	average
maximum load	maximum
minimum load	minimum
voltage over crack	average
reference voltage	average
maximum voltage of crack detection gauge 1	maximum
maximum voltage of crack detection gauge 2	maximum
stress intensity factor range	average
crack length from Johnson formular	average
laboratory temperature	average
temperature of the specimen	average
temperature of the climate chamber	average
temperature of the load cell	average

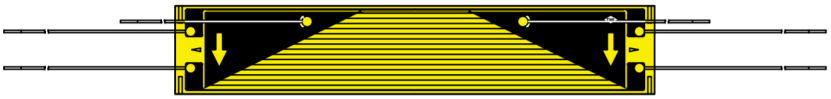

Figure 3.7 FAC-5 Tokyo Sokki Kenkyujo [29]

3.7 Crack detection gauges

For crack length detection and defined crack length FAC-5 Tokyo Sokki Kenkyujo crack detection gauges (CDG) were used. The gauges were glued on the specimens surface in a distance of 2 mm from the tip of the machined notch. The strips consist of a thin wire mesh enclosed in a film, Figure 3.7 shows one such stripe.The CDG´s were positioned in a way the fine grid runs perpendicular to the crack. When the crack passes one of the conductor path and cut it, the crack detection gauge is changing its resistance. The crack detection gauges were connected to a pre-resistor, which was connected to the measuring amplifier. The wires fail one after the other, this leads to a step shape of the measured value, so that the failure of each wire can be identified individually. Through the position of the CDG and the number of steps, the current position of the crack on the surface can be determined. The CDG's used had a measurement width of 4.5 mm with a conductor spacing of 0.1 mm.

3.8 PT100 Thermocouple

For determination of the Temperature PT100 thermocouple in four wire technology were used. Four PT100 sensors were used to determine the temperature at several points. In the climate chamber one sensor were fixed by a magnet on the specimens surface. One was measuring the temperature at the bottom of the climate chamber. For determination of the outside temperature one sensor was placed next to the measuring amplifier. The fourth sensor was stick by a magnet next to the load cell of the resonant testing machine. The temperature sensor next to the load cell of the resonant testing machine and the PT100 which was measuring the temperature on the specimen were calibrated by the ice water method.

3.9 Temperature correction of the load cell

The load cell of the resonant pulsing machine was not insulated for cold temperatures. A change of the temperature was influencing the measured force. To determine the magnitude of the influence, the chamber was cooled down without s sample. The load cell was located outside the temperature chamber, the results measured during the test are shown in Figure 3.8. The influence on the measured force is intolerable, a linear fit mapping is in good agreement with the measured values 3.8. Formula 3.1 corrects the

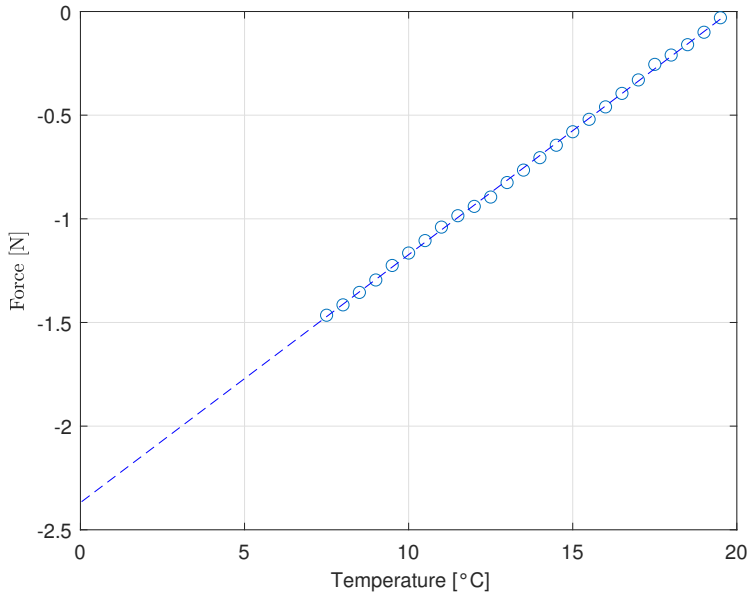

Figure 3.8 Fit of temperature and measured force

temperature influence and was used for the load setting of the pulser. The value $T_{loadcell}$ is the temperature of the load cell.

$$f_{korr} = -0.1196 T_{loadcell} + 2.3689 \tag{3.1}$$

Chapter 4

Calibration curves for different temperatures

The Johnson equation is investigated for a long time [28, 26] and has already been used in previous experiments at TUHH [15]. The use of other materials and a different temperature range requires the re-validation of the equation. To determine the quality of the Johnson formula, tests were carried out for the two types of material.

The equation is compared with the values of the Crack Detection Gauges and the beachmarks. For comparison the results are plotted in normalized form.
On Y-axis the crack voltage is normalized with the voltage at reference time. The X-Axis shows the crack length normalized with the width of the specimen. The three lines are the three values which are compared. The red line are the normalized values of the Johnson equation. In magenta the standardized mean values of the Crack detection gauges are shown. The crackling by Crack Detection Gauges is corrected for the non-straight crack-front by the beachmarks. The blue circles are the beachmarks, which have a fitted curve in blue.
The following parameters were used for the experiments on the calibration curves. The ultimate stress ratio was subsequently $R = 0.5$ and $R = 0.75$ for the beachmarks. This correspond to the force of $\sigma_{max} = 80$ KN and $\sigma_{min} = 40$ KN for the crack growth and $\sigma_{max} = 80$ KN and $\sigma_{min} = 60$ for the creation of the beachmarks.
The experiments were performed for different temperatures. The creation of Calibration Curves for all Temperatures that are performed in later experiments would have been to extensive. For the calibration curves the following temperatures were selected: Room Temperature($\sim$19°C), 0°C, -50°C and -80°C.
The accuracy refers to the range of the normalized crack length that was examined for the following experiments. The accuracy refers to the method of photographs determination.

For low temperatures this accuracy can not be assumed and must be investigated.

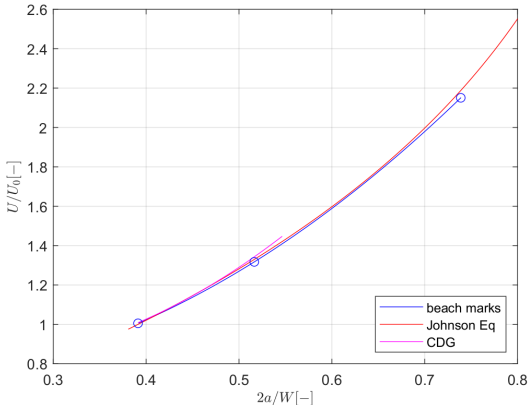

(a) Room temperature

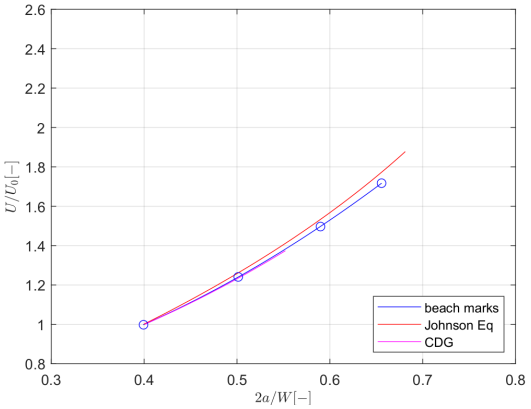

(b) -20°C

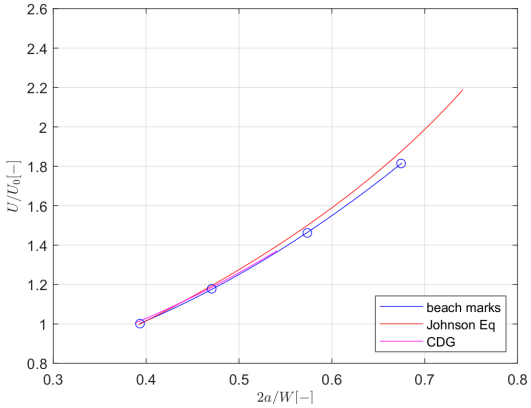

(c) -50°C

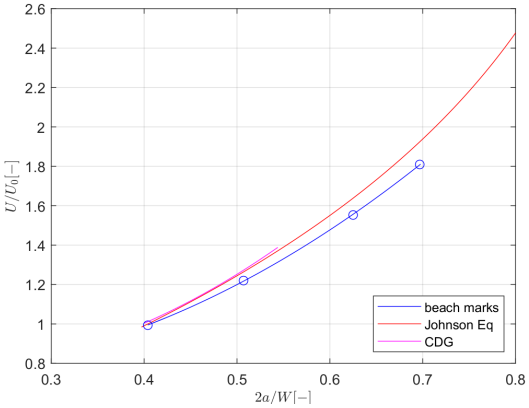

(d) -80.

Figure 4.1 Calibration curves of S500 steel for the tested temperatures.

4.1 Calibration curves of S500 steel

For the S500 steel specimen experiments have been performed for the determination of the calibration curves. As mentioned before the tested temperatures are room temperature, 0°C, -50°C and -80°C. The diagrams of the normalized calibration curves are shown in the Figure 4.1. The diagram for room temperature is shown in Figure 4.1a the agreement between the Johnson equation and the fitted curve of the beach marks is very good. The average percentage deviation is 0.61 the maximum percentage deviation is less than 1%. According to Figure 4.1b the deviations rise to 1.24% (average value) and 2.42% (maximum value). The change in correspondence of the envelopes from -20 to -50 degrees is small. The average deviation is 1.26%, the maximum deviation is 2.51%. For -80°C the deviations are almost doubled. The mean accuracy is 97.94 the biggest difference the is lower 5%.

The temperature of the specimen has a significant influence on the accuracy of the Johnson-Equation. For the S500 base-material specimens a decrease of accuracy can be easily noticed for lower temperatures.

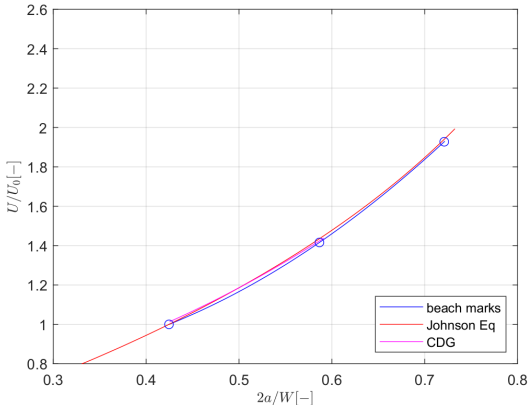

(a) Room temperature

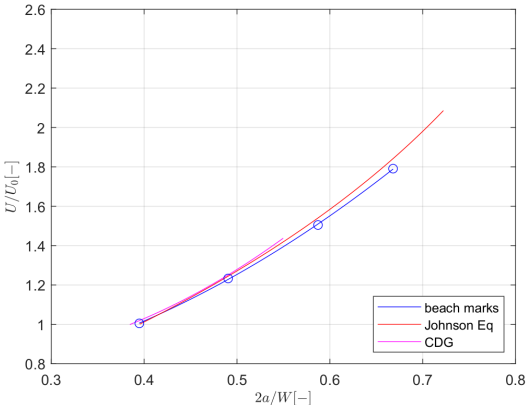

(b) -20°C

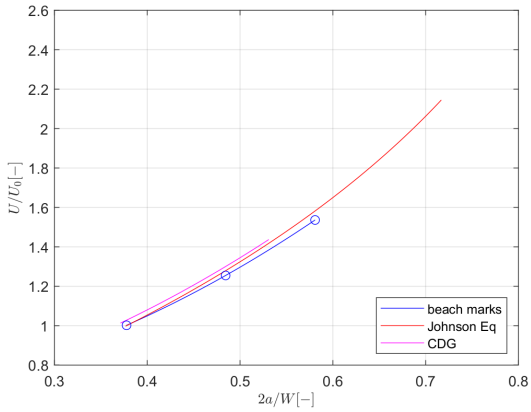

(c) -50°C

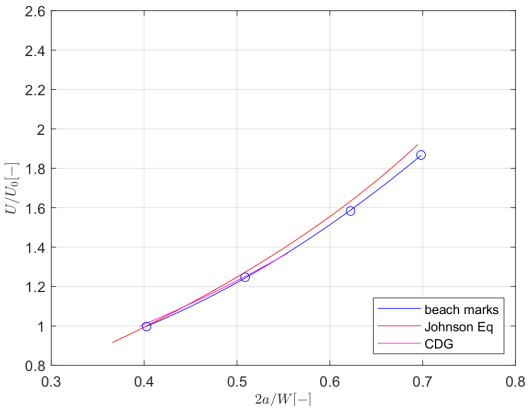

(d) -80.

Figure 4.2 Hier fehlt noch der beschreibende text zu den kalibrierungslinien

4.2 Calibration curves of welded S500 steel

The calibration curves of the welded specimen are shown in Figure 4.2. At the room temperature the accuracy of Johnson - Equation was verified by the fitted curve of the benchmark. The maximum discrepancy of the curves is 1.72% where the mean deviation is 0.86% (Figure 4.2a). With lower temperatures the accuracy decreases. For -20°C(fig.4.2) the average discrepancy is 0.99% and maximum is about 2.08%. The curves for -50°C are plotted in Figure 4.2c. The discrepancies are very similar to the curves at -80°C. For both temperatures the average value of difference is 1.35%, The maximum discrepancies are 2.90% and 2.69% for the temperature of -50°C and -80°C respectively.

4.3 Conclusion

At room temperature there is a very good agreement between Johnson equation and beachmarks for both tested materials. With lower temperatures there is a trend of lower accuracy of the Johnson equation for both materials. For the base material at -80°C there is higher loss of accuracy, whereas the results of welded specimen for -50°C and -80°C are similar.

The absolute discrepancies are plotted in Figure **??** a for the homogeneous S500 steel and in Figure **??**b for the welded specimens. ???I am working on this Figure, it was not good with absolute values!??? The error is growing with the distance to the start-crack-length, which makes sense, cause this value is predefined. In curves for ??? the kinks are marking the position where the curves of beachmark and Johnson equation are crossing. The trend is that the Johnson-Equation become less accurate as the temperatures decreases. The data for benchmarks were obtained experimentally too, which means that the evaluation can cause discrepancies as well.

At room temperature and -50°C on the welded specimen only three beachmarks has been placed during calibration-experiments, while for the other experiments four beachmarks was generated. This has an impact on the number of nodes of the fitting function and in consequence on the fitted function itself. In summary, the curves show a sufficient accuracy for the evaluation of the crack length for the folowing experiments.

Chapter 5

Decreasing ΔK Experiments

For the investigations of fatigue crack growth rates from threshold area to Paris region the decreasing ΔK method is chosen. The fatigue crack growth for a certain stress intensity factor range can be determined. The experiment is described in ASTM 647-2015 [13]. For the experiments which are the basis of this work a stress intensity range of R=0.5 is chosen. The experiment is started for a given stress intensity factor range. Equation 5.1 is taken from ASTM-647-2015 and describes the stress intensity factor.

$$\Delta K = \frac{\Delta P}{B}\sqrt{\frac{\pi\alpha}{2W}sec(\frac{\pi\alpha}{2})} \tag{5.1}$$

with the normalised crack length $\alpha = 2a/W$ and force range $\Delta P = P_{max} - P_{min}$

Equation 5.1 is valid for this setup with clamped specimen.

The testing machine operates during a working cycle with a constant force range ΔP.

The fatigue crack growth rate can be determined for the cycle by using equation 5.2 the change of the crack length da of the Johnson equation and the number of Cycles N. The stress intensity factor range is growing with rising crack length. The nominal ΔK is determined for each cycle(see figure 5.1).

$$(da/dN)_a = (a_{i+1} - a_i)/(N_{i+1} - N_i) \tag{5.2}$$

For the next cycle the force range is reduced by a constant stress ratio of R=0.5. The method is called stepped force shredding and the accompanying reduction of the stress intensity factor range is shown in Figure 5.1. The reduction of the stress is a sensible task. On the one hand, the stress intensity factor range is growing with increasing crack length, this has to be considered for the choice of the loads of the next run . On the other hand, the plastic zone size in the crack-tip has to be considered, for smaller ΔK the plastic zone size is shrinking. For this reason the crack has to grow out of the plastic zone that was created during the previous run. Only after that the crack growth values are

valid for the actual run. The ASTM 647 - 2015 [13] recommends a reduction of the force of maximum 10% and minimum crack growth of 0.25 mm per load step. The end of the experiment is reached, when the fatigue crack growth rate is lower than 10^{-7} [mm/cycl]. For runs between 10^{-6} [mm/cycl] and 10^{-7} [mm/cycl] at least five values of equi-distant ΔK are recommended.[13] Undergo this crack growth rate is marking the threshold stress intensity factor range.

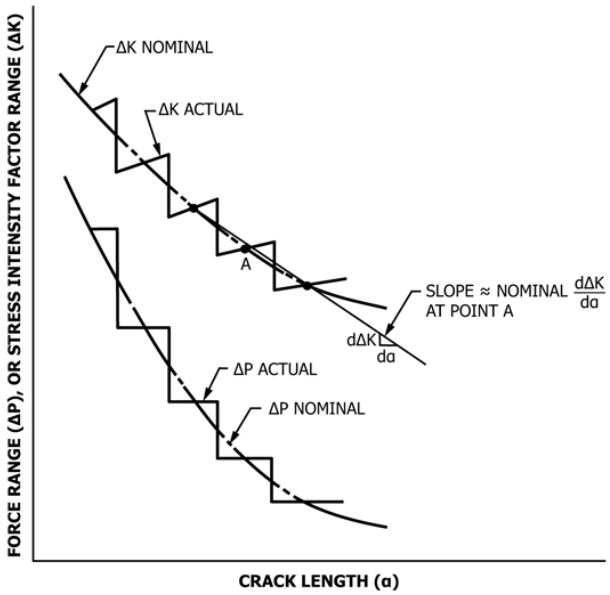

Figure 5.1 Reduction of load range ΔP and resulting stress intensity range ΔK during decreasing ΔK-method [13]

The decreasing-ΔK-experiments were conducted for specimen of both materials. To eliminate the influence of the machined notch the decreasing ΔK-experiment is started after a specified crack length is reached. For the determination of the start-crack-length for the Johnson-equation and the start of the experiment the crack detection gauges were used on the specimens. The results of the decreasing Δk method specimen are plotted as ΔK over da/dN (see Figures 5.2 and 5.4). Each point represents one work-cycle of the experiment. The blue line shows the fit of the Paris region and threshold region of stress intensity factor in two stages. The values between 10^{-6}[mm/cycl] and 10^{-7} [mm/cycl] are fitted separately. The intersection of the fit and $10^{-}7$ [mm/cycl] leads to the threshold value ΔK_{th}

5.1 Results for S500 steel

The results of the S500 base material steel specimen are plotted in Figure 5.2. For the stable crack growth area, the fitted line has a slope of 3.3843. The threshold value ΔK_{th} results in 3.85 MPA$\sqrt{m}$.

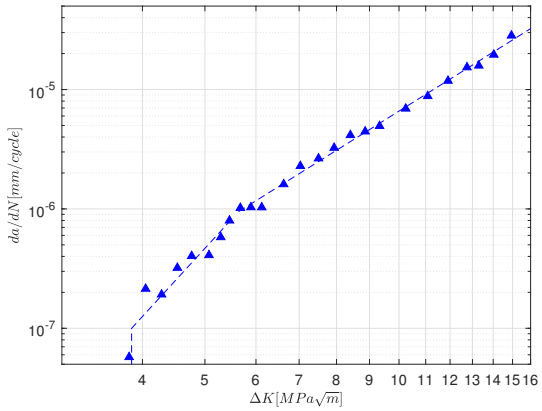

Figure 5.2 Results of the Decreasing ΔK experiment of the base material specimen.

The results of the experiments were compared with the results of Zerbst et. al [31]. The threshold stress intensity factor of Zerbst et al. is between $3MPA\sqrt{m}$ and $3.5MPA\sqrt{m}$ which is slightly higher than the results of the experiments. The influence of different yield strengths of steels is a minor factor on the crack growth behaviour [27].

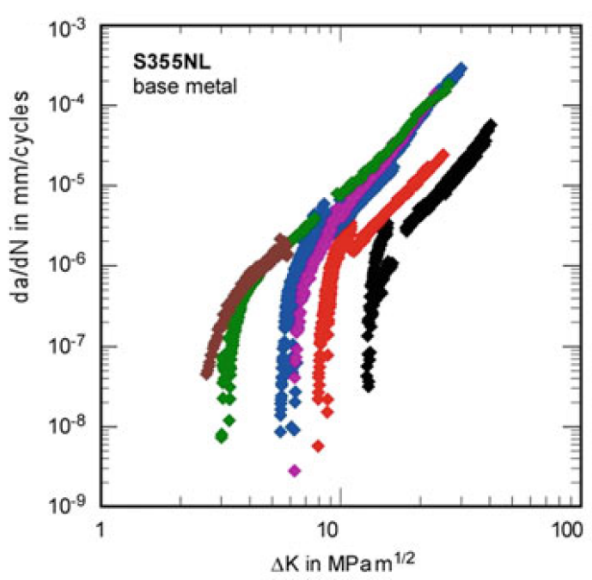

Figure 5.3 Results of the Decreasing ΔK test of S355NL steel. The green squares are the results for R=0.5 taken from [31]

5.2 Results for welded S500 steel

The results of the welded S500 steel specimen are plotted in Figure 5.4. For the stable crack growth the slope of the fitted line is 2.36. The evaluation of the threshold value of the stress intensity factor range results in $\Delta K_{th} = 2.3585\ MPA\sqrt{m}$.

The comparative data from Ohta at al. presented in Figure 5.5 shows a good agreement between the experimental data. The threshold value ΔK_{th} of Ohta is between

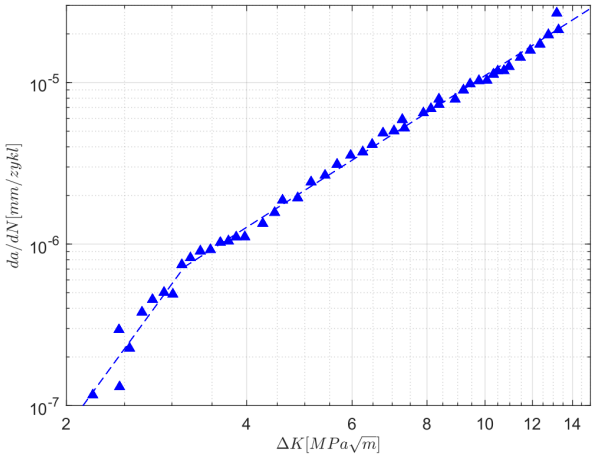

Figure 5.4 Results of the Decreasing ΔK experiment of the welded specimen.

2.0 $MPa\sqrt{m}$ and 2.5 $MPa\sqrt{m}$, the value of the experiment is 2.35 $MPa\sqrt{m}$. For $10^-5mm/cylce$ the points of the experiment are in the region of 10 $MPa\sqrt{m}$ while for the same value Ohtas results are between 10 and 10.5 $MPa\sqrt{m}$ and gradients of the fits are similar.

British Standard (BS) is giving recommendations for crack growth law for steel in air in BS 7910 2013 [9].

For welded joints the recommendations for a two stage curve at stress ratio of $R \geq 0.5$ are given in table **??**. For comparison the curve is plotted in Figure **??**.

British Standard 7910 2013	
$\Delta K_{th} = 63$ N/mm$^{3/2}$	Stage A/Stage B transition point $\Delta K = 144$ N/mm$^{3/2}$
Stage A	$A_1 = 2.10 \cdot 10^{-17}$ $m = 5.10$
Stage B	$A_2 = 1.29 \cdot 10^{-12}$ $m = 2.88$

Table 5.1 Recommendations of stress intensity factor curves of BS and IIW valid for $R \geq 0.5$.

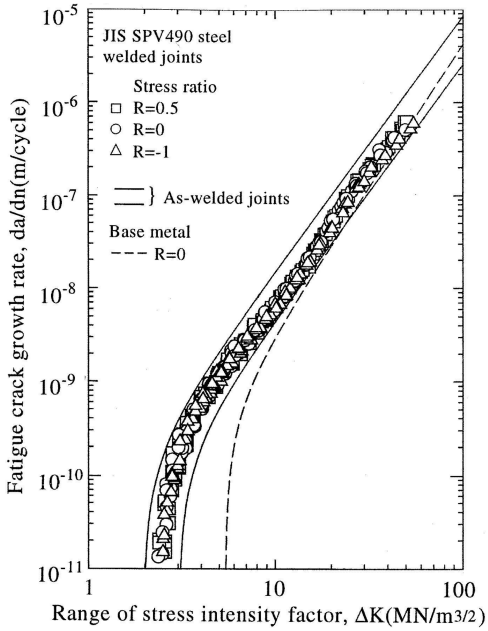

Figure 5.5 Results of the Decreasing ΔK experiment for the welded S500 steel by Otha et al. 1997.

5.3 Conclusion

Concluding the results of the decreasing ΔK experiments are showing a good agreement with literature. The strong influence of the stress ratio is visible in Figure 5.3. For this reason only experiments with the same stress ratio are point of interest. The slopes of the crack growth curve are similar for the experiments and from literature. The threshold values for crack arrest of the experiments are close to literature considering that they are data from experiments. For the welded specimen the deformation because of the welding process was not measured before testing.

??? Vergleich der Versuchsergebnisse mit Kurven von BS oder Ohta ???

Chapter 6

Crack propagation in cold environment

The increased use of steel in structures in arctic regions makes it necessary to investigate crack growth behaviour in cold environment. For lower temperatures ferrite steel can show a change in crack growth behaviour. Several sources reported decreasing crack growth rates for lowering temperatures and a sudden increase of crack growth at a certain temperature .[Quellen]

The results are then compared with literature values

Rolof had investigated the FDBT-temperature for the same material by Charpy impact tests. The results of these experiments are shown in chapter **??**. The investigations will be used for the evaluation of the experiments of this thesis too.

???Fatigue tests for decreasing temperatures by Stephens and Chang 1980 are showing a trend of decreasing crack growth rates until 90 °K is reached and the crack growth rates are increasing???.

???

Chapter 7

Constant ΔK experiments

In this thesis the crack growth rates for cracks in S500 steel and the material of welded joints are investigated. The experiments for generation of the whole curves are very expensive, therefore the scope of the investigations is reduced. For a reduction of time and costs not complete da/dN versus ΔK curves for different temperatures were generated in this work. Just one experiment for each material was conducted. The specimens were tested for decreasing temperatures but constant stress intensity factor ΔK and stress ratio R.
The tests were started at room temperature, for a stress intensity ratio of $\Delta K = 8MPA\sqrt{m}$ and a stress ratio of $R = 0.5$. After a load block was completed, a marker with a limit stress ratio of $R = 0$ is applied to the fracture surface.

Afterwards, the temperature in the climate chamber was reduced and waited until the target temperature was reached. This procedure was repeated down to a temperature of -100 °C for the WM and -110 °C for the BM. To determine the applied load to reach the stress intensity factor range of 8 $MPA/\sqrt{m}$ the crack length was required. For this reason the Johnson crack length was implemented in the measuring software and allowed to follow the value of crack length while the experiment was running.

7.1 Results of basematerial specimen

In the Figure 7.1 the results of the experiment for the S500 base material were presented. The obtained crack growth rates are plotted over the applied temperature. For each point the scatter band of the crack growth rate for mild carbon steel is given according to Barsom and Rolfe [3].

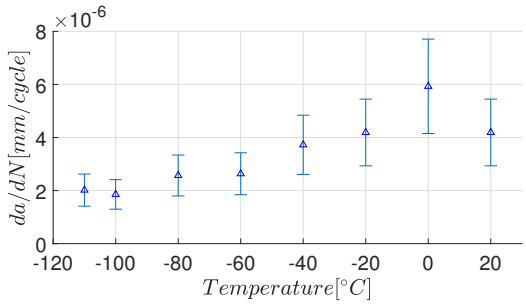

Figure 7.1 Results of the constant ΔK experiment of base material specimen. The crack growth is plotted over the temperature.

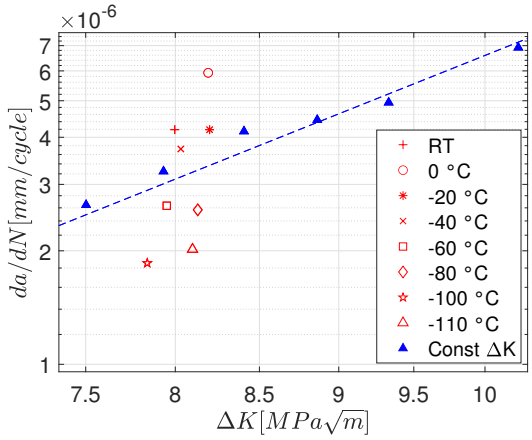

Figure 7.2 Results of the decreasing ΔK experiment at RT and for const ΔK of 8 MPA $\sqrt{m}$ for different temperatures.

The results of the BM specimen are shown in Figure 7.1 plotted as crack growth rate over temperature. For -20°C and -40°C the crack growth rate is rising from 4.19E-6 mm/-cycle at room temperature to 5.93E-6 mm/cycle. According to the scatter bands these fluctuations are within the range of the expected uncertainty. The increase of the value was related to the uncertainty of the experiment.

For lower temperatures the curve is falling constantly to a crack growth rate of 1.85E-6 mm/cycle at -100 °C. Plotting the same values into the da/dN versus ΔK Diagram is shown in Figure 7.2. The results of the constant ΔK experiment at RT is in good agreement with the result of the decreasing ΔK experiment at room temperature for $8MPA/\sqrt{m}$. For the experiments with the BM specimen the target value of ΔK was matched for all temperatures at the experiment.

7.2 Results of welded specimen

The experiment of the crack in the welded joint is plotted in Figure 7.3. The trend of the crack growth rates is showing a similar behaviour as the specimen from BM. For lower temperatures the crack growth rate is reduced. In Figure 7.4 the results of constant ΔK

experiments are plotted together with the results of decreasing ΔK experiment. Some differences between the results of the constant ΔK experiment and crack growth rate from the decreasing ΔK experiment might be noted. For welded specimens there are many factors such as defects in the material and welding distortions that effects the results.
The welding distortion for the specimen used for the decreasing ΔK experiment was not estimated before it was tested. For this reason, no conclusion can be drawn about the influence of geometry on the results. ???Evtl möglichkeit rissfronten vergleichen? The effects of the resulting differences in geometry were not taken into account during evaluation. The prediction of the crack length during the experiment was not as precise as in the first experiment which leads to a SIF that was not as close as the results of BM test to the target value.

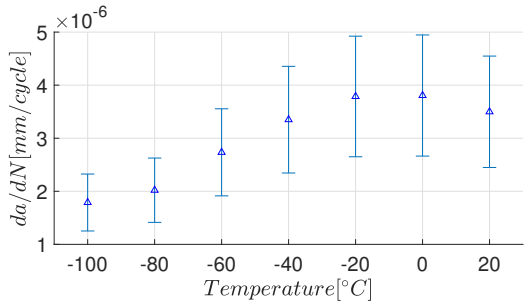

Figure 7.3 Results of the constant ΔK experiment of welded specimen.

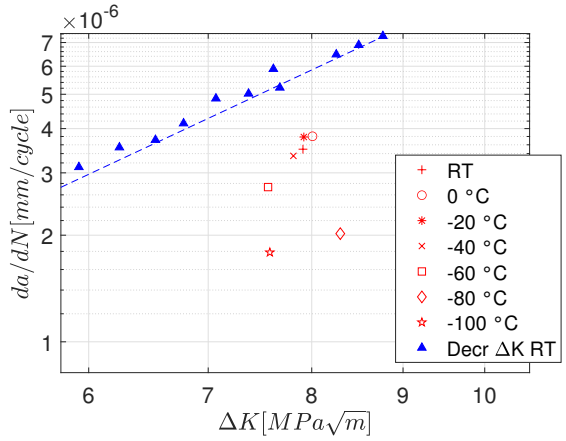

Figure 7.4 Results for the welding material of the const ΔK experiment for low temperatures plotted together with. the decreasing ΔK experiment at RT.

This becomes obvious when values was plotted together with the results of the decreasing ΔK experiments in Figure 7.4. The discrepancies between the SIF of the experiment are higher than for the basematerial.

7.3 Results of the Charpy tests

Charpy impact test were performed for the same materials by Rolof. [16] The V-notch was placed in the S500 base material and in the but-joint. The experiments were carried

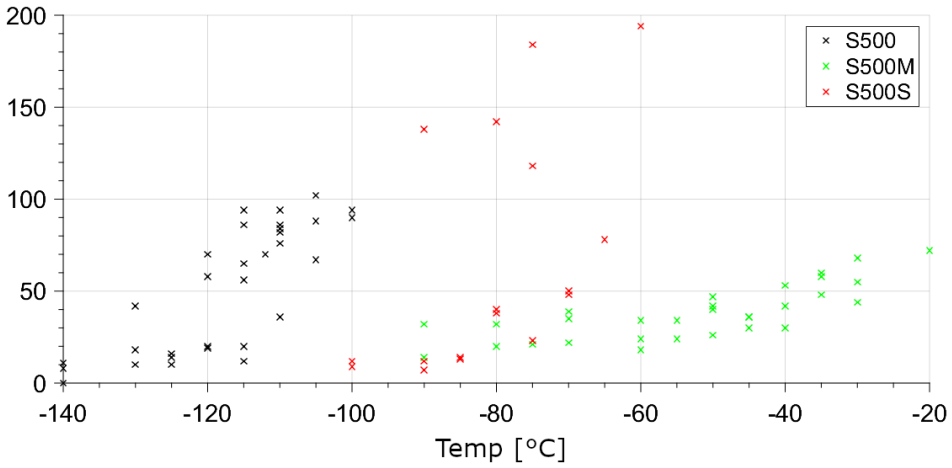

Figure 7.5 Charpy impact tests for S500 base material, heat affected zone (S) and material of welded joint (M) by Rolof [16] The Charpy impact energy is plotted over the temperature.

out over a temperature range from -100°C and -140°C for the S500 basematerial and -20°C to -90°C for the butt-joint specimens. In Figure 7.5 the results of the experiments were plotted, the results for the base material was plotted in grey as S500, the but joint as S500M in green.

The data from the experiment was evaluated by Rolof. The T_{27J} temperature for Charpy Impact Energy was estimated using different methods and fits. ???The results of SINTAP procedure of British Steel [10] were compared for different fitting functions.??? A polynomial approach of the form $f(x) = p_1 x + p_2$ and an exponential approach of the form $f(x) = a * exp(bx)$ were compared. The results for the T_{27J} are presented in table 7.1.

Table 7.1 Results for T_{27J} Charpy Impact Energy according to SINTAP by Rolof [16].

fitting	S500 BM	S500 WM
	T_{27J} [°C]	T_{27J} [°C]
exp	-127.56	-63.54
poly	-120.67	-43.84
conservative exp	-119.09	-47.25
conservative poly	-115.17	-36.60
mean exp	-126.91	-63.11
mean poly	-120.96	-44.97

The transition-temperature T_{27J} is defined for a Charpy impact energy of 27 Joule. The interpolation of the values leads to values between -120°C and -130°C??? for the S500 basematerial and -44°C and -64°C?? for the welded joint. The complete SINTAP

curves are shown in the ???appendix???. The degree of determination for the specimen of the welded joint is $R^2 = 0.5642$. The largest deviation for the basematerial is 6.89 °C??. Another criterium, that is regarded qualitative, for the determination of the brittle temperature is the $T_{B50\%}$ criterium. The brittle temperature is reached by this criterium if the crack surface is dominated by brittle crack surface. In the author's opinion, the temperature of the base material is in good agreement with the Charpy experiment. For the welded specimen the transition temperature seem to occur for lower T_{27J} than for the Charpy experiments. [16]

7.4 Discussion

At cold temperatures, two effects compete for dominance under the influence of cyclic loads on steel [24].
On the one hand the yield strength is increasing with lower temperatures. It causes a decrease of the plastic zone size in the crack tip and a sinking crack growth rate. [1]
On the other hand static modes like cleavage cracking and microvoid coalescence can be activated[32]. For temperatures below FDBT it can cause an abrupt increase of the crack growth rates because of the occurrence of static modes or cyclic cleavage. [1]

7.4.1 Base material specimen

Walters et al. [30] tested crack growth behaviour for S460 in cold environment and compared it with the results from Charpy tests. According to the results of the Charpy test the Charpy energy of 27 J was reached at −79 °C. The temperature T_{J46}=−73 °C is responding to a Charpy energy of 46 Joules. The Charpy test is explained in chapter 2.8.
Walters investigations were conducted for temperatures between RT and -120 °C. A stress range of R=0.1 was applied during the experiments the results for the experiments with SIF ranges of 8 $MPa\sqrt{m}$ and 12 $MPa\sqrt{m}$ are shown in Figure 7.6.
In the opinion of the authors the FTT cannot be determined exactly due to the scattering of the data in the transition area. Concluding to their opinion the T_{27J} and T_{46J} temperatures are a good indicators of the region not for the exact position of the fatigue ductile brittle transition. What is more, it was pointed out that the FTT could be slightly higher than according to these values.

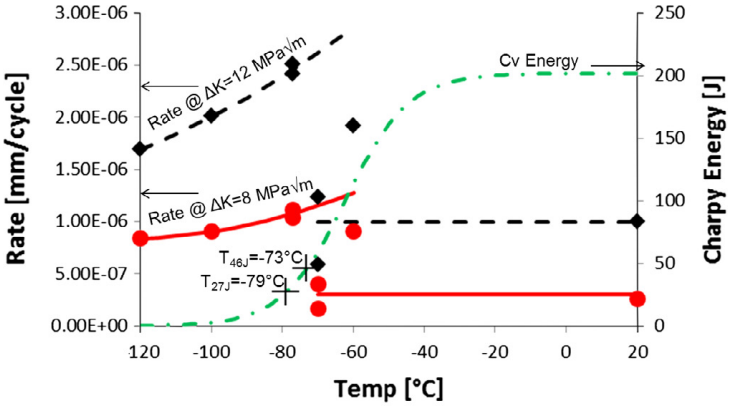

Figure 7.6 Results from crack growth rates and and Charpy test at low temperatures. The Red curve is representing a SIF of 8 $MPa\sqrt{m}$ Taken from [30]

According to the results presented in Chapter **??** for S500 specimen the crack growth values are decreasing constantly for temperatures from 0°C to -110°C. The results of the Charpy tests of Rolof [16] for the same material are giving a T_{27J} range from -115 °C to -130 °C. However, the scattering of the results is high and makes an accurate determination of the fracture brittle temperature impossible.
Zhao et al.[32] had investigated the influence of the temperature on the hardness of the material and the slope of Paris equation for DH 36 steel. The results of his experiments were represented by the fatigue crack growth rate for lower temperatures is decreasing until FTT is reached. The authors detected also an relationship between lgC and m and temperature. For temperatures above FTT m value was decreasing while lgC was increasing. By reaching the FTT this trend was reversed. The occurrence of FTT in this region was confirmed by SEM images.

???Walters and Zhao are predicting on the results of Charpy the FTT higher than the DBTT.??? Walters expect a difference of about 18 °C between T_{27J} and FTT. Zhao´s investigations lead to a higher difference of 30 °C.

???The experiments can neither confirm nor rebut differences in this heigh between the FTT and DBT.??? The results of the Charpy fracture to brittle tests are showing the transition point in a range from -115 °C to -130°C. The fatigue tests were performed up to a temperature of -110 °C and no brittle caused change resulting higher crack growth rate have been detected.

7.4.2 Welded specimen

For the crack growth in weld material the trend of decreasing values for lower temperatures was observed as well. This trend did not change even after decreasing the temperature below T_{27J}. For the tested temperature range of RT to -100 °C the welded material is not showing the behaviour of FDBT in the crack growth.
Zhao et al. [33] had investigated the fatigue crack propagation of a butt weld in DH36 steel. The crack plane was in the fusion zone of base material and butt weld. For tem-

perature of -60 °C compared to RT a reduced crack growth was observed. The Vickers hardness was showing a growth for fusion zone and welding line as well for low temperatures. The Vickers hardness and fatigue crack was correlated at low ΔK. It was discovered that the microstructure and the chemical compensation is having a big impact on the fatigue behaviour. For stable propagation stages the fractography evaluation of the crack surfaces were confirming this results.

Alvaro et al. [2] had tested weld material SENB specimens for fatigue crack growth at low temperature. In his studies he had mentioned FDBT for for temperatures of -80 °C and lower. Figure 7.7 is showing the results of decreasing ΔK for different temperatures.

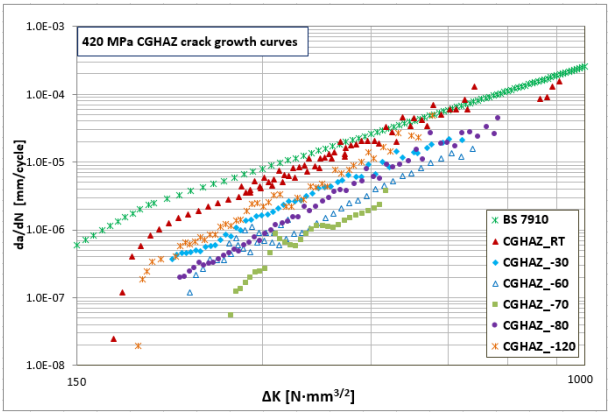

Figure 7.7 Results of the decreasing ΔK experiment of as welded S460 by Alvaro et al. for different temperatures.[2]

From RT to -70°C temperature the crack growth rates were constantly decreasing. For -80 °C the crack growth rates were higher than for -70 °C. For -120 °C the crack growth rates raised again. This leads to the conclusion that FTT was in the region of -80°C. The results of decreasing ΔK tests at 8 $MPA\sqrt{m}$ were compared with the results of Charpy tests. Two types of Charpy specimen was taken into account. The point of interest was the V-Notched specimen as used by Rolof [16]. Figure 7.8 is showing the results of Charpy test decreasing ΔK test plotted over the temperature. On the left axis the Charpy energy is plotted on the right the crack growth rates for 8 $MPA\sqrt{m}$. For the V-Notched Charpy specimen Alvaro estimated the DBT transition temperature T_{27J} at -55°C. Comparison of the values of Charpy test T_{27J} and FTT of crack propagation test showed a difference of 25°C.

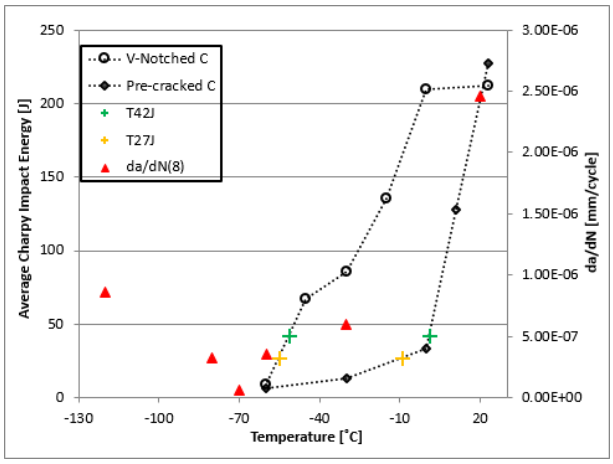

Figure 7.8 Crack growth rates for SIF of 8 $MPa\sqrt{m}$ plotted together with results of Charpy test.[2]

Comparing this results with the results of Rolof [16] and welded specimen constant ΔK test of this thesis the difference is even bigger. During constant ΔK at -100°C no DFBT had occurred which is a difference higher 35 °C compared to the results of Rolof. Walters [30] had pointed out the high scattering of crack growth testing in the transition region which could be one of the possible reason however many other factors can have an impact to the fatigue ductile to brittle behaviour. Some of them that are expected to cause such as descripencies are the test conditions with focus on the used specimen geometry and the load ratio. The weld material is not free free defects and inhomogeneities as well. The process of welding itself and the reheating when welds has more than one layer have an impact on microstructure and mechanical properties [20]. The used welding components have a big impact on the microstructures and shape of lattice too [22].
???Concluding there is a lot of work to do in this subject. Many experiments had done for high SIF even if in practical use lower SIF are applied.???

Chapter 8

Summary and Conclusion

The main objective of this work was investigations of the crack growth behaviour of steel and welded joints at low temperatures. The effect of ductile to brittle temperature is well examined for fracture but recently rediscovered for fatigue. For this reason the experiments for crack growth were carried out in the Laboratory

The experiments were carried out with center notched specimens tested on a cyclic testing machine. A climate chamber for controlled temperature was build around the specimen. For the determination of the crack length the direct current drop method has been used.

First the accuracy of the Johnson equation has been estimated by creating calibration curves at room temperature and below. The accuracy of the Johnson equation was found to be satisfactory.?

Next part of the research was the investigations into the crack growth rates at room temperatures. The experiments with a stepwise reduction of the stress intensity factor were carried out and the results were plotted in da/dN versus ΔK diagrams, the Paris region was fitted and the threshold value was estimated.

With the results for base material and welded joint the stress intensity range of 8 $MPa\sqrt{m}$ have been estimated the following experiments. For this value the crack growth rates for temperatures between RT and -100°C for the welded material between RT and -110°C for base material have been estimated. The results have been compared with Charpy tests. For present study the fatigue ductile brittle transition had not been noticed within the reached temperatures. Nevertheless, the results are in agreement with the current state of the art.

-Experiment with constant SIF of 8 MPa$\sqrt{m}$ have been carried out with the same specimen for different temperatures. In particular for welded material this is reducing the influence of different geometry and microstructure when more than one specimen is used. Experiments of other authors i found have been carried out with one specimen for different SIF at the same temperature. For other temperatures an other specimen had

been used.

-First experiments with M(t) specimen which are directly comparing S500 steel and the material of a welded joint.???Hier noch Verhalten von M(T). alle anderen ct und senb, antonio hat mt abe rnur schweißssimuliert

-The results were compared with results of charpy test where the specimen was made from the same material charge.

-The results are to be explained with the investigations of other authors. But the fatigue transition temperature have not be reached during the experiments that is why the conclusions cannot be definitively verified.

-A disadvantage of testing crack growth rates at low temperatures like in this thesis is that the information about the slope of the Paris fit can not be calculated. For investigations for one SIF do not allow conclusions on the values for other SIF.

-The scattering in the transition region is quite high, more points at a temperature are delivering a higher accuracy.

Chapter 9

Future work

A future task is to continue the experiments with the remaining M(t) specimens. In particular, experiments with temperatures below the FTT would be a consistent step to verify the conclusions reached in this thesis.

The influence of the specimen geometry on the results would be an interesting task. Most other experiments of this topic have been made with compact tension specimen and Single-Edge-Notched Bend Specimen. Which may not reflect the load cases of structures as good as M(t) specimen.

The influence of the welding distortion on the results of the experiment may be higher than of other specimen geometries. For this reason the influence of the welding distortions on crack growth rates should be investigated.

The temperature regulation of the climate chamber is not the perfect solution. For very low temperatures opening the valve for the nitrogen causes temperature fluctuations in the chamber. An adjustable valve with a constant gas flow would reduce this problem.

Bibliography

[1] A. Alvaro, O. Akselsen, X. Ren, A. Kane: Fundamental Aspects of Fatigue of steel in Arctic Applications. In: ISOPE-2014 Busan ; conference proceedings ; the proceedings of The Twenty Fourth (2014) International Ocean and Polar Engineering Conference, Busan, Korea, June 15 - 20, 2014 ; includes [papers from 11] symposia as part of the conference, S. 247–254

[2] A. Alvaro, O. Akselsen, X. Ren, G. Perillo, B. Nyhus: On the Relation between Fatigue and Static Ductile to Brittle Transition for Weld Simulated 420 MPa Structural Steel. Cupertino, California, USA : International Society of Ocean and Polar Engineers (ISOPE), 2017 (The proceedings of the Twenty-seventh (2017) International Ocean and Polar Engineering Conference). – ISBN 9781880653975

[3] Barsom, John M. ; Rolfe, Stanley T.: Fracture and fatigue control in structures: Applications of fracture mechanics. 2. ed. Englewood Cliffs, NJ : Prentice-Hall, 1987 (Prentice-Hall international series in civil engineering and engineering mechanics). – ISBN 0133298639

[4] Bock und Polach, R. U. F. ; Klein, Marco ; Kubiczek, Jan ; Kellner, Leon ; Braun, Moritz ; Herrnring, Hauke: State of the Art and Knowledge Gaps on Modelling Structures in Cold Regions. In: Volume 8: Polar and Arctic Sciences and Technology; Petroleum Technology, American Society of Mechanical Engineers, 06092019. – ISBN 978–0–7918–5887–5

[5] Braun, Moritz ; Scheffer, Robert ; Fricke, Wolfgang ; Ehlers, Sören: Fatigue strength of fillet–welded joints at subzero temperatures. In: Fatigue & Fracture of Engineering Materials & Structures 43 (2020), Nr. 2, S. 403–416. http://dx.doi.org/10.1111/ffe.13163. – DOI 10.1111/ffe.13163. – ISSN 8756758X

[6] Braun, M., Milakovic, A.-S., Andresen-Paulsen, G., Fricke, W., and Ehlers, S: A novel approach to consider misalignment effects in assessment of fatigue tests. In: Ship Technology Research, submitted for publication

[7] Braun, M., Milakovic, A.-S., Ehlers, S., Kahl, A., Seidel, M., and Fischer, C.: Sub-zero temperature fatigue strength of butt-welded normal and high-strength steel joints for ships and offshore structures in Artic regions: ASME 2020

39th International Conference on Ocean, Offshore and Arctic Engineering, Fort Lauderdale, FL, USA

[8] Braun, M., Milakovic, A.-S., Renken, F., Fricke, W., and Ehlers, S.: Application of Local Approaches to the Assessment of Fatigue Test results obtained for Welded Joints at Sub-Zero Temperatures: submitted for publication. In: International Journal of Fatigue, submitted for publication

[9] British Standard Institution: Guide to methods for assessing the acceptability of flaws in metallic structures: BS 7910:2013+A1:2015. Dec 2013

[10] British Steel ; British Steel (Hrsg.): SINTAP: Structural Integrity Assessment Procedures for European Industry. Sheffield, UK,

[11] Dowling, Norman E.: Mechanical behavior of materials. 4th ed., International ed. Boston : Pearson, 2013. – ISBN 0273764551

[12] E08 Committee: Test Method for Linear-Elastic Plane-Strain Fracture Toughness KIc of Metallic Materials

[13] E08 Committee: Test Method for Measurement of Fatigue Crack Growth Rates

[14] European Space Agency: Satellites witness lowest Arctic ice coverage in history. http://www.esa.int/Applications/Observing_the_Earth/Envisat/Satellites_witness_lowest_Arct

[15] F. Sallaba: Analysis of fatigue crack growth threshold of welded structural steel. Projectthesis

[16] Franziska Anke Rolof: Bewertung der Kerbschlagzähigkeit verschiedener Zonen geschweißter Konstruktionen. Hamburg,

[17] Fricke, Wolfgang: Lectures on fatigue strength of ships and offshore structures. Hamburg, December 2017

[18] Gautier D. et al.: Assessment of undiscovered oil and gas in the Arctic. In: Science (New York, N.Y.) 324 (2009), Nr. 5931, S. 1175–1179. http://dx.doi.org/10.1126/science.1169467. – DOI 10.1126/science.1169467

[19] Göpfrich, Josef: Fatigue crack growth rate measurements in GL D36 grade welded structural steel: Masterthesis. http://dx.doi.org/10.15480/882.1654. Version: 2018

[20] Gubeljak, N. ; Legat, J. ; Koçak, M.: Effect of fracture path on the toughness of weld metal. In: International Journal of Fracture 115 (2002), Nr. 4, S. 343–359. http://dx.doi.org/10.1023/A:1016368019571. – DOI 10.1023/A:1016368019571. – ISSN 03769429

[21] Hochfellner, Veronika: Investigation of constraint effect on fatigue crack growth rate measurements: Masterthesis

[22] J. Park, M. K.: Investigation of fatigue and fracture characteristics for low temperature metals considering the effect of various alloying components

[23] Milakovic, A.-S., Braun, M., Willems, T., Hendrikse, H., Fischer, C., and Ehlers, S.: Methodology for estimating offshore wind turbine fatigue life under combined loads of wind, waves and ice at sub-zero temperatures. 2019

[24] N. R. Moody, W. W. Gerberich: Fatigue crack propagation in iron and two iron binary alloys at low temperatures. In: Materials Science and Engineering 41 (1979), Nr. 2, S. 271–280. http://dx.doi.org/10.1016/0025-5416(79)90148-4. – DOI 10.1016/0025–5416(79)90148–4. – ISSN 0025–5416

[25] National Snow and Ice Data Center: That's a wrap: A look back at 2019 and the past decade. http://nsidc.org/arcticseaicenews/. Version: 2020

[26] Petersen ; Belloni, G. ; Gariboldi, E. ; Lo Conte, A. ; Tono, M. ; Speranzoso, P.: On the Experimental Calibration of a Potential Drop System for Crack Length Measurements in a Compact Tension Specimen. In: Journal of Testing and Evaluation 30 (2002), Nr. 6, S. 11149. http://dx.doi.org/10.1520/JTE12346J. – DOI 10.1520/JTE12346J. – ISSN 00903973

[27] Schijve, Jaap: Fatigue of structures and materials. [Online-ausg.]. Dordrecht : Kluwer Academic, 2001. – ISBN 0–7923–7013–9

[28] Schwalbe, Karl-Heinz ; Hellmann, Dieter: Application of the electrical potential method to crack length measurements using Johnson's formula. Geesthacht, (GKSS E)

[29] Tokyo Sokki Kenkyujo: Fac-5 Crack detection gauge. https://tml.jp/e/product/strain_gauge/fac_list.html. Version: 28.01.2020

[30] Walters, Carey L. ; Alvaro, Antonio ; Maljaars, Johan: The effect of low temperatures on the fatigue crack growth of S460 structural steel. In: International Journal of Fatigue 82 (2016), 110–118. http://dx.doi.org/10.1016/j.ijfatigue.2015.03.007. – DOI 10.1016/j.ijfatigue.2015.03.007. – ISSN 01421123

[31] Zerbst, Uwe (Hrsg.) ; Madia, Mauro (Hrsg.) ; Schork, Benjamin (Hrsg.) ; Hensel, Jonas (Hrsg.) ; Kucharczyk, Pawel (Hrsg.) ; Ngoula, DesireTchoffo (Hrsg.) ; Tchuindjang, Didi (Hrsg.) ; Bernhard, Julian (Hrsg.) ; Beckmann, Carla (Hrsg.): Fatigue and Fracture of Weldments. Cham : Springer International Publishing, 2019. http://dx.doi.org/10.1007/978-3-030-04073-4. http://dx.doi.org/10.1007/978-3-030-04073-4. – ISBN 978–3–030–04072–7

[32] Zhao, Weidong ; Feng, Guoqing ; Ren, Huilong ; Leira, Bernt J. ; Zhang, Ming: Temperature–dependent characteristics of DH36 steel fatigue crack propagation. In: Fatigue & Fracture of Engineering Materials & Structures 15 (2019), S. 889. http://dx.doi.org/10.1111/ffe.13177. – DOI 10.1111/ffe.13177. – ISSN 8756758X

[33] Zhao, Weidong ; Feng, Guoqing ; Zhang, Ming ; Ren, Huilong ; Sinsabvarodom, Chana: Effect of low temperature on fatigue crack propagation rates of DH36 steel and its butt weld. In: Ocean Engineering (2019), S. 106803. http://dx.doi.org/10.1016/j.oceaneng.2019.106803. – DOI 10.1016/j.oceaneng.2019.106803. – ISSN 00298018